THE JOURNAL OF
PHYSICAL CHEMISTRY
LETTERS
A JOURNAL OF THE AMERICAN CHEMICAL SOCIETY

September 15, 2022
Volume 13
Number 36
pubs.acs.org/JPCL

ACS Publications
Most Trusted. Most Cited. Most Read.

www.acs.org

THE JOURNAL OF PHYSICAL CHEMISTRY LETTERS
A JOURNAL OF THE AMERICAN CHEMICAL SOCIETY

pubs.acs.org/JPCL Letter

Manifesting Direction-Specific Complexation in $[HFIP_{-H}{\cdot}H_2O_2]^-$: Exclusive Formation of a High-Lying Conformation

Jia Han, Lei Wang, Wenjin Cao, Qinqin Yuan, Xiaoguo Zhou,* Shilin Liu, and Xue-Bin Wang*

Cite This: J. Phys. Chem. Lett. 2022, 13, 8607−8612 Read Online

ACCESS | Metrics & More | Article Recommendations | Supporting Information

ABSTRACT: Size-selective, negative ion photoelectron spectroscopy in conjunction with quantum chemical calculations is employed to investigate the geometric and electronic structures of a protype system in catalytic olefin epoxidation research, that is, deprotonated hexafluoroisopropanol ($[HFIP_{-H}]^-$) complexed with hydrogen peroxide (H_2O_2). Spectral assignments and molecular electrostatic surface analyses unveil a surprising prevalent existence of a high-lying isomer with asymmetric dual hydrogen-bonding configuration that is preferably formed driven by influential direction-specific electrostatic interactions upon H_2O_2 approaching $[HFIP_{-H}]^-$ anion. Subsequent inspections of molecular orbitals, charge, and spin density distributions indicate the occurrence of partial charge transfer from $[HFIP_{-H}]^-$ to H_2O_2 upon hydrogen-bonding interactions. Accompanied with electron detachment, a proton transfer occurs to form the neutral complex of $[HFIP{\cdot}HOO^{\bullet}]$ structure. This work conspicuously illustrates the importance of directionality encoded in intermolecular interactions involving asymmetric and complex molecules, while the produced hydroperoxyl radical $HOO^{\bullet}$ offers a possible new pathway in olefin epoxidation chemistry.

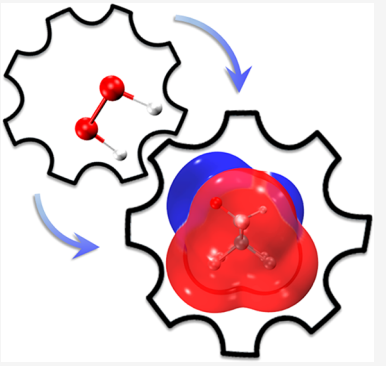

Epoxides have been widely exploited in synthetic chemistry as a result of three extraordinary properties offered by the three-membered oxirane ring—high reactivity toward nucleophiles, synthetic flexibility, and capability of achieving atom economy in an efficient and selective fashion.[1,2] Great interest has been focused on utilizing epoxides as special intermediates in various chemical and medicinal opportunities, such as enantioselective synthesis and production of pharmaceutical drug precursors.[3−5] The high demand of epoxide-related compounds has stimulated their large-scale manufacture, in which olefin epoxidation has been identified as one main synthetic route.[6]

Catalytic oxidation of olefins to produce epoxides commonly takes place in the presence of oxidants such as peroxomonosulfate,[7] percarbonic acids,[8] or hypochlorites,[9] which inevitably produces large amounts of chemical waste byproducts and is thus not economically promising. Hydrogen peroxide (H_2O_2), as an affordable and environmentally benign oxidant,[10] provides an attractive option for alkene epoxidation, which, however, requires additional catalysts mostly associated with transition-metal oxides to be electrophilically activated.[11,12] Additionally, the immiscibility of H_2O_2 with nonpolar olefins in organic medium presents another major drawback.[13,14]

Fluorinated alcohols are a class of extraordinary organic solvents with powerful dissolving ability while maintaining water-soluble properties.[15−19] Perfluorinated alcohols, particularly 1,1,1,3,3,3-hexafluoroisopropyl alcohol (HFIP) and 2,2,2-trifluoroethanol (TFE), were applied as solvents to catalytically activate H_2O_2 in the absence of any metal oxides, permitting selective epoxidation of alkenes and Baeyer−Villiger oxidation of ketones.[20,21] A dramatic acceleration of reaction rates (up to 5 orders of magnitude) for olefin epoxidation with H_2O_2 in HFIP was reported.[22] Computational modeling suggested a boosted electrophilic activation of H_2O_2 arisen from aggregated HFIP H-bond networks[23] and revealed an intriguing solvent microstructure with a triphilic character in which fluorous, polar, and nonpolar moieties segregate albeit with macroscopical homogeneity.[24]

While it has been proposed that olefin epoxidation proceeds via electrophilic H_2O_2 catalytically boosted by HFIP, other mechanistic scenarios may concurrently exist, for example, via a nucleophilic pathway that involves negatively charged $[H_2O_2{\cdots}HFIP]$ complexes.[12] Hereby, we carry out negative ion photoelectron spectroscopy (NIPES) combined with theoretical calculations on a well-defined model system, that is, deprotonated HFIP ($[HFIP_{-H}]^-$) complexed with H_2O_2. Our study aims at (1) identifying crucial intermolecular interactions between HFIP solvent and H_2O_2 oxidant at the molecular level, (2) obtaining geometric and electronic structures of the $[HFIP_{-H}{\cdot}H_2O_2]^-$ complex, and (3) probing electron-coupled proton transfers that commonly occur in catalytic oxidation reactions.

Received: July 18, 2022
Accepted: August 16, 2022
Published: September 8, 2022

https://doi.org/10.1021/acs.jpclett.2c02237
J. Phys. Chem. Lett. 2022, 13, 8607−8612

Figure 1 shows the 20 K NIPE spectrum of $[HFIP_{-H}\cdot H_2O_2]^-$ obtained at 193 nm (6.424 eV), along with that of the

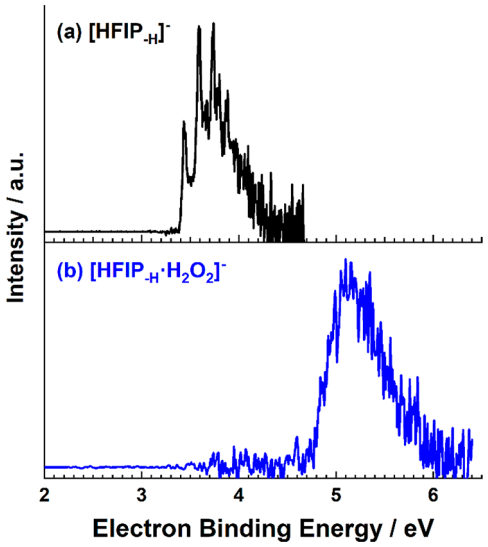

Figure 1. Experimental low-temperature photoelectron spectrum of $[HFIP_{-H}]^-$ at 266 nm (4.661 eV) (a) and $[HFIP_{-H}\cdot H_2O_2]^-$ at 193 nm (6.424 eV) (b).

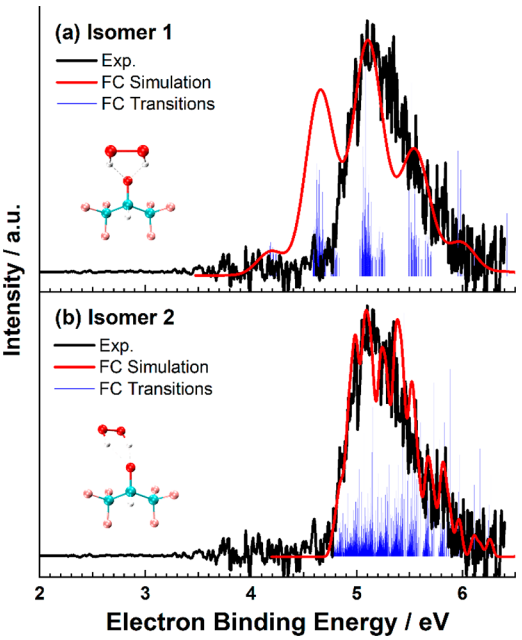

Figure 2. FCFs simulated spectra of isomer 1 (a) and isomer 2 (b). The experimental spectrum is presented as well for comparison. (insets) The optimized anion structures (see Figure S2 for details).

isolated $[HFIP_{-H}]^-$ anion obtained at 266 nm (4.661 eV) for comparison (the 193 nm spectrum of $[HFIP_{-H}]^-$ was reported previously[25]). The adiabatic detachment energy (ADE) and vertical detachment energy (VDE) of $[HFIP_{-H}\cdot H_2O_2]^-$ are determined from the onset threshold and maximum of the spectral band to be 4.78 and 5.10 eV, respectively, indicative of a moderate geometry change upon photoelectron detachment. This band bears a similar spectral profile compared to that of $[HFIP_{-H}]^-$ (Figure 1a) but blue-shifted in ADE by 1.35 eV. It is also apparent that, while the falling tail of the complex anion is parallel to that in $[HFIP_{-H}]^-$, the rising edge is broader and much less-resolved (see Figure S1 for an overlay comparison), suggesting more geometric rearrangements during electron detachment for the complex anion.

It is well-known that H_2O_2 has three conformers in the gas phase, namely, *gauche* (nonplanar), *cis* (planar), and *trans* (planar), in which the nonplanar *gauche* geometry is most stable.[26] Therefore, combining a *gauche* H_2O_2 molecule with the $HFIP_{-H}$ moiety was initially adopted in geometry optimization for the complex. Figure S2 displays low-lying ωB97XD/jun-cc-pVTZ optimized anion and neutral structures along with their relative Gibbs free energies computed at the DLPNO−CCSD(T)/aug-cc-pVTZ level including zero-point energy (ZPE) corrections. To our surprise, all low-lying anion complex structures eventually converged into configurations with $HFIP_{-H}$ moiety binding to *cis*-H_2O_2, characterized by forming double hydrogen bonds. Isomer 1 (see also the inset in Figure 2a) possesses C_s symmetry, with two identical hydrogen bonds (1.778 Å) formed between two hydrogen atoms of H_2O_2 and the oxygen atom of $HFIP_{-H}$ anion, producing a symmetrical five-membered ring structure. In contrast, isomer 2 (the inset in Figure 2b) features an asymmetrical arrangement with longer hydrogen bond lengths (1.796 and 1.792 Å) than in isomer 1, in which one of the hydrogen atoms of H_2O_2 binds to the oxygen atom of $HFIP_{-H}$ anion in the symmetry plane of the $HFIP_{-H}$ part, while the other approaches the oxygen atom in a significantly distorted manner. Isomer 1 is the most stable, owing to the strong stabilization that stemmed from the symmetrical and compact hydrogen-bonding network, while isomer 2 is higher in Gibbs free energy by 0.92 (1.33) kcal/mol at 300 (20) K.

Upon electron detachment, proton transfer from H_2O_2 to $HFIP_{-H}$ concomitantly occurs in both isomeric forms, producing a new configurational motif in which the $HOO^\bullet$ radical interacts with the HFIP molecule in a synclinal (SC) conformation for isomer 1, while in an antiperiplanar (AP) structure for isomer 2 (Figure S2). It is worth noting that the energetic order of two conformational isomers flips over after the excess electron is removed; that is, the isomer 2 HFIP(AP)·HOO complex is lower in Gibbs free energy by 0.04 (0.47) kcal/mol than isomer 1 HFIP(SC)·HOO at 300 (20) K. This energetic ranking for the neutral complex can be rationalized in a well-accepted scenario where the gaseous AP conformer is more stable than SC for HFIP molecule.[27]

Based on those optimized anion and neutral geometries, theoretical VDEs are calculated at the DLPNO−CCSD(T)/aug-cc-pVTZ level to be 5.18 and 5.09 eV for isomers 1 and 2, respectively, both congruent with the experimental value of 5.10 eV, particularly for isomer 2 (Table S1). The predicted ADEs are, however, much smaller than the experimental ADE by ∼1.6 eV, due to large anion-to-neutral geometry changes accompanied with proton transfer and, consequently, the negligible 0−0 transition intensity from the anion to the neutral. In this context, the experimentally determined ADE is regarded as an upper limit of true ADE value. It is interesting to note that anion isomer 2, which is less stable, provides the best VDE match to the experiments (5.09 vs 5.10 eV). Therefore, the contribution of isomer 2 should not be excluded, simply because it would have a negligible equilibrium population within the cryogenic ion trap. In our previous photoelectron spectroscopy study of the Gly·I^- complex,[28] we have successfully detected isomers with significantly higher energy of 3.93 kcal/mol than the most stable structure, demonstrating that the species with higher relative energy

https://doi.org/10.1021/acs.jpclett.2c02237
J. Phys. Chem. Lett. 2022, 13, 8607−8612

formed in an ambient electrospray ionization (ESI) source can be kinetically trapped and isolated, which further leads to the populations inconsistent with the Boltzmann distribution law at low temperatures.

A thermochemistry analysis for the transformation pathway from anion isomer 1 to isomer 2 together with the structure of the transition state (TS) is presented in Figure S3. The thermodynamic barrier for isomer 2 rearranging to isomer 1 via the rotation of the H_2O_2 moiety around the oxygen atom on $HFIP_{-H}$ is estimated to be 1.63 kcal/mol at room temperature. Trapping the energetically less-favorable isomer 2, initially generated under ambient ESI conditions, is therefore feasible considering the insufficient energy provided by environments to overcome the interconversion barrier and the rapid solvent evaporation and collisional cooling in the cold ion trap.

To facilitate differentiating contributions from both isomers, the Franck−Condon factors (FCFs) and FC spectrum of each were computed. Figure 2 compares the experimental and FC simulated spectra for both isomers, with the predominant FC transitions noted as blue-colored sticks. Extensive vibrational excitations on multiple vibrational modes (Figure S4) are expected in view of the evident geometry rearrangement upon electron detachment. The major vibrational progressions for FC transitions prevailingly involve the hydroxyl hydrogen atom, that is, O−H stretching and C−O−H bending and wagging motions, consistent with the predicted proton transfer during the photoelectron detachment process. Despite engaging the same set of atoms, FC calculations yield dramatically different spectral patterns with distinct vibrational progressions for different isomers. The FC spectrum of isomer 1, dominated by the O−H stretching mode, provides a poor match to the experimental spectrum. In contrast, the simulated spectrum of isomer 2, derived from excitations of complex combination bands, agrees much better with the measured one, even reproducing the discernible vibrational structures along the rising edge of the spectrum. Apparently, isomer 2 of high energy contributes dominantly if not exclusively to the experiments, clearly violating the expected isomeric population based on the Boltzmann distribution law. This surprising result certainly warrants further investigation as followed up below.

To address how H_2O_2 orientates itself in approaching the $[HFIP_{-H}]^-$ anion, we turn to examine the anion moiety electrostatic surface, which has been widely accepted as an effective way to analyze and predict direction-specific noncovalent interactions.[29−31] In $[HFIP_{-H}]^-$, negative electrostatic potential (ESP) sweeps for any given region owing to the presence of an extra electron.[32] Accordingly, the most negative area is anticipated to have the highest possibility to interact favorably with electrophiles. As shown in Figure 3a, the global minimum of ESP on the molecular surface, calculated to be −141.5 kcal/mol, exactly resides near the oxygen atom in the symmetry plane, suggesting a tendency for H_2O_2 binding to take place in this direction. Indeed, for both anionic complex isomers, the positive sites of the H_2O_2 molecule interact attractively with the most negative region on the $[HFIP_{-H}]^-$ anion, consistent with the expectation from the long-range electrostatic attraction viewpoint.

Bearing in mind that, when a molecule approaches another molecule or ion at a distance close enough, they begin to interact with each other, and this subsequently results in immediate perturbations on the molecule's electrostatic potential, derived from the electric field of the other entity.[33−37] Thereby the concept of "average local ionization energy (ALIE)" kicks in to take orbital interactions into account. The region on a molecular surface with the lowest value of ALIE represents the site of least tightly held electrons, in which electrophilic substitution, protonation, and free radical attack preferably occur.[38,39] Three local minima of ALIE cover the surface area around the regioselectivity domain described by electrostatic potential in $[HFIP_{-H}]^-$ (Figure 3b). Unlike the global minimum point of ESP that locates approximately along the C−O bond axis, the lowest magnitude of ALIE ($\bar{I}_{min}$, 108.1 kcal/mol) has shifted off this axis toward the lower tip of the oxygen atom (the direction here is based on the orientation as drawn in Figure 3), followed by two symmetric local minima with weaker reactivity (112.2 kcal/mol) on either side of the molecular symmetry plane. The position of $\bar{I}_{min}$ in Figure 3b matches well with the observed favorable site of the complexation motif between H_2O_2 and $[HFIP_{-H}]^-$ shown as isomer 2 in Figure S2 (side view of isomeric geometries are available in Figure S5 for clearer illustration). This lower-tip guidance as the primary reactive site versus upper-tip allows for the contacting spot, initially falling onto the most negative zone on the ESP surface, to slide downward to form the first H bond. By anchoring to the lower side, the second intermolecular H bond can be captured in a configuration involving one of the unoccupied ALIE local minima on the upper region. Therefore, the dominant binding pocket, featuring two asymmetrical H-bond docking sites as in the anionic isomer 2, was finally accessed through reorienting the H-bond donor following the guidance of ESP and subsequently the ALIE. The combination of these two theoretical descriptors provides an extraordinary view on how the two species dock together and how this docking arrangement is correlated to the reaction coordinate that ultimately leads to complexation as isomer 2, albeit with a higher energy. The proposed direction-specific reactivity warrants further exploration to define general conditions under which this mechanism can be uniformly operative.

A distance-dependent ESP is scrutinized to elucidate the origins of the excess electron in the $[HFIP_{-H}{\cdot}H_2O_2]^-$ complex (Figure S6). As the one thing approaches the other, a small

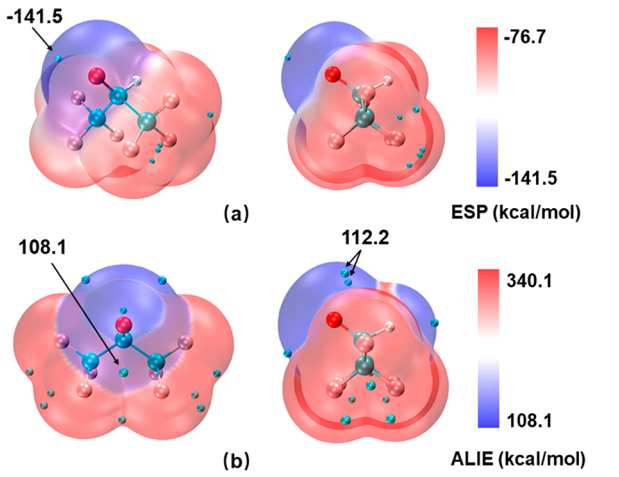

Figure 3. (a) Electrostatic potential (ESP) on the molecular surface of the $[HFIP_{-H}]^-$ anion, computed on the 0.001 au contour of the electron density; (b) ALIE on the molecular surface of the $[HFIP_{-H}]^-$ anion, computed on the 0.001 au contour of the electron density. Blue dots designate the location of corresponding global minima and local minima.

https://doi.org/10.1021/acs.jpclett.2c02237
J. Phys. Chem. Lett. 2022, 13, 8607−8612

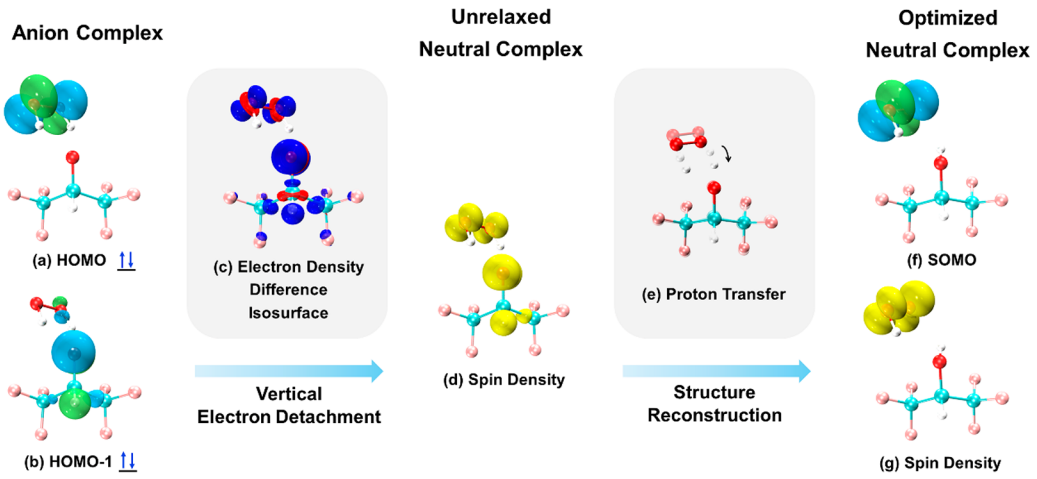

Figure 4. Electronic structure information from the anion to neutral complex: molecular orbital pictures for the HOMO (a) and HOMO−1 (b) of $[HFIP_{-H}{\cdot}H_2O_2]^-$; electron density difference mapping upon vertical electron detachment, in which red and blue isosurfaces denote increasing and decreasing in electron density, respectively (c); spin density distribution of the unrelaxed neutral complex (d); illustration of proton transfer process upon electron detachment (e); molecular orbital picture for the SOMO (f) and spin density distribution (g) of optimized [HFIP·HOO•] neutral.

portion of the excess charge clearly spreads over from the oxygen atom of $[HFIP_{-H}]^-$ to both oxygen atoms in H_2O_2. In the optimized anion complex, the negative charge expands onto all three oxygen atoms with comparable ratios; thus, it can be imagined that the electron detachment occurs from those three oxygens. The Merz−Singh−Kollman (MK) and Natural Population Analysis (NPA) atomic charge distributions (Table S2) further demonstrate quantitatively that the photodetached electron can be traced to both $[HFIP_{-H}]^-$ and H_2O_2 moieties with nearly equivalent contributions, in line with the qualitive conjecture based on ESP surface calculations (detailed analysis is available in Supporting Information). After the electron detached, one of the H atoms originally on the H_2O_2 side readily relocates to the $HFIP_{-H}$ without any energy barrier, producing HOO• and HFIP both in the neutral state.

The highest occupied molecular orbitals (HOMO and HOMO−1) of $[HFIP_{-H}{\cdot}H_2O_2]^-$ of isomer 2, the dominant contributor to the experiments, are depicted in Figure 4. The HOMO of $[HFIP_{-H}{\cdot}H_2O_2]^-$ is a π^* antibonding orbital residing on the H_2O_2 unit, while the HOMO−1 consists of a lone-pair p-orbital on O and an s-orbital on the H of $HFIP_{-H}$. Given that the energy difference between the HOMO and HOMO−1 is relatively small (0.32 eV), it is conceivable that the electron signal recorded in experiments is attributed to transitions from both orbitals, in line with the conclusions drawn from ESP and charge distribution analyses that electron detachment takes place on both parts in the complex.

Figure 4c illustrates the electron density difference between the anion and the unrelaxed neutral, aiming at intuitively revealing the regions where electron density ρ increases or decreases (red or blue isosurfaces) upon vertical photoelectron detachment. Electron density depletions around three oxygen atoms and the H atom of $HFIP_{-H}$ are explicitly reproduced, substantiating that the detached electrons are from p-orbitals on three O atoms in combination with an s-orbital on the H atom of $HFIP_{-H}$, congruent with the spin density map shown in an unrelaxed neutral complex (Figure 4d). The singly occupied molecular orbital (SOMO) and spin density for the relaxed neutral complex after the proton transfer are shown in Figure 4f,g. The SOMO is disclosed to be composed of the same atomic orbitals as the HOMO of $[HFIP_{-H}{\cdot}H_2O_2]^-$, that is, p-orbitals of two O atoms on HOO, and the unpaired spin density is contributed primarily by SOMO, both indicative of formation of hydroperoxyl radical HOO•. The final product following photodetachment of $[HFIP_{-H}{\cdot}H_2O_2]^-$ leads to the [HFIP·HOO•] radical complex that can be regarded as the HOO• radical loosely complexed with the HFIP molecule, enabling the potential recyclability for HFIP reuse.

In conclusion, we reported an integrated NIPES and theoretical study of $[HFIP_{-H}{\cdot}H_2O_2]^-$, aiming to characterize the geometries and electronic structures of both anion and neutral complexes. Detailed FC analyses and comparison with the experimental spectrum reveal a surprising dominance of an asymmetric, high-lying hydrogen-bonded isomer, even at low-temperature conditions. This abnormal observation highlights an interesting complexation process that is driven by direction-specific electrostatic attractions en route to H_2O_2 approaching $[HFIP_{-H}]^-$, as visualized by ESP and ALIE molecular surface calculations. Qualitive ESP and quantitative charge analyses suggested a significant charge transfer from $[HFIP_{-H}]^-$ to H_2O_2 neutral moiety upon dual H-bonds formation, leading to delocalized distributions of the excess negative charge over three oxygen atoms. The origins of detached electrons were determined to be derived from both $HFIP_{-H}$ and H_2O_2 parts. Such an electron detachment is seen to induce a proton relocation from H_2O_2 to $[HFIP_{-H}]^-$, giving rise to the formation of hydroperoxyl radical HOO• that is weakly bound to an HFIP molecule. These insights for a protype system in catalytic epoxidation research convey valuable fundamental understandings to better elucidate the complicated catalytic reaction mechanisms. Moreover, the generation of the HOO• radical promises a new direction for future research advancement on developing an alternative strategy for olefin epoxidation.

■ ASSOCIATED CONTENT

Supporting Information

The Supporting Information is available free of charge at https://pubs.acs.org/doi/10.1021/acs.jpclett.2c02237.

https://doi.org/10.1021/acs.jpclett.2c02237
J. Phys. Chem. Lett. 2022, 13, 8607−8612

Experimental methods and theoretical details; Overlay comparison of experimental $[HFIP_{-H}]^-$ and $[HFIP_{-H}\cdot H_2O_2]^-$ spectra (Figure S1); Low-lying, ωB97XD/jun-cc-pVTZ optimized isomers for the $[HFIP_{-H}\cdot H_2O_2]^-$ anion and corresponding neutral with their relative Gibbs free energies at 300 K (Figure S2); Schematic free energy diagram for the transformation between anion isomer 1 and isomer 2 at 300 K (Figure S3); Predominant vibrational excitations of each neutral complex (isomer 1, 2) and corresponding vibrational frequencies (Figure S4); Side view of average local ionization energies (ALIE) on the molecular surface of the $[HFIP_{-H}]^-$ anion computed on the 0.001 au contour of the electron density, geometries of anionic isomer 2 and isomer 1 (Figure S5); Electrostatic potentials (ESP) snapshots on the molecular surface during formation of $[HFIP_{-H}\cdot H_2O_2]^-$ complex at different ion−molecule distances with both constituents adopting the geometries in the optimized anion complex, computed on 0.001 au electron density contour (Figure S6); Experimental and calculated adiabatic (ADEs) and vertical detachment energies (VDEs) for $[HFIP_{-H}\cdot H_2O_2]^-$ complex anion (Table S1); Merz−Singh−Kollman (MK) and Natural Population Analysis (NPA) atomic charge distributions for $[HFIP_{-H}\cdot H_2O_2]^-$ anion and corresponding neutral complex at both unrelaxed and optimized geometries (Table S2) (PDF)

AUTHOR INFORMATION

Corresponding Authors

Xiaoguo Zhou − *Hefei National Laboratory for Physical Sciences at the Microscale, Department of Chemical Physics, University of Science and Technology of China, Hefei, Anhui 230026, P. R. China;* orcid.org/0000-0002-0264-0146; Email: xzhou@ustc.edu.cn

Xue-Bin Wang − *Physical Sciences Division, Pacific Northwest National Laboratory, Richland, Washington 99352, United States;* orcid.org/0000-0001-8326-1780; Email: xuebin.wang@pnnl.gov

Authors

Jia Han − *Hefei National Laboratory for Physical Sciences at the Microscale, Department of Chemical Physics, University of Science and Technology of China, Hefei, Anhui 230026, P. R. China*

Lei Wang − *Hefei National Laboratory for Physical Sciences at the Microscale, Department of Chemical Physics, University of Science and Technology of China, Hefei, Anhui 230026, P. R. China*

Wenjin Cao − *Physical Sciences Division, Pacific Northwest National Laboratory, Richland, Washington 99352, United States;* orcid.org/0000-0002-2852-4047

Qinqin Yuan − *Physical Sciences Division, Pacific Northwest National Laboratory, Richland, Washington 99352, United States; Department of Chemistry, Anhui University, Hefei, Anhui 230601, P. R. China*

Shilin Liu − *Hefei National Laboratory for Physical Sciences at the Microscale, Department of Chemical Physics, University of Science and Technology of China, Hefei, Anhui 230026, P. R. China*

Complete contact information is available at: https://pubs.acs.org/10.1021/acs.jpclett.2c02237

Notes

The authors declare no competing financial interest.

ACKNOWLEDGMENTS

This work was supported by U.S. Department of Energy (DOE), Office of Science, Office of Basic Energy Sciences, Division of Chemical Sciences, Geosciences, and Biosciences, and performed using EMSL, a national scientific user facility sponsored by DOE's Office of Biological and Environmental Research and located at Pacific Northwest National Laboratory, which is operated by Battelle Memorial Institute for the DOE. The financial support of the National Natural Science Foundation of China (No. 21873089 and 22073088) is gratefully acknowledged too. The quantum chemical calculations were performed on the supercomputing system in the Supercomputing Center of the University of Science and Technology of China.

REFERENCES

(1) Padwa, A.; Murphree, S. S. Epoxides and Aziridines- A Mini Review. *Arkivoc* **2006**, *3*, 6−33.

(2) de Souza, R. O. M. A.; Miranda, L. S. M.; Bornscheuer, U. T. A Retrosynthesis Approach for Biocatalysis in Organic Synthesis. *Chem. - Eur. J.* **2017**, *23*, 12040−12063.

(3) He, J.; Ling, J.; Chiu, P. Vinyl Epoxides in Organic Synthesis. *Chem. Rev.* **2014**, *114*, 8037−8128.

(4) de Vries, E. J.; Janssen, D. B. Biocatalytic Conversion of Epoxides. *Curr. Opin. Biotechnol.* **2003**, *14*, 414−420.

(5) North, M.; Pasquale, R.; Young, C. Synthesis of Cyclic Carbonates from Epoxides and CO_2. *Green Chem.* **2010**, *12*, 1514−1539.

(6) Yan, Z.; Tian, J.; Wang, K.; Nigam, K. D.; Luo, G. Microreaction Processes for Synthesis and Utilization of Epoxides: A Review. *Chem. Eng. Sci.* **2021**, *229*, 116071.

(7) Liu, T.; Zhang, D.; Yin, K.; Yang, C.; Luo, S.; Crittenden, J. C. Degradation of Thiacloprid via Unactivated Peroxymonosulfate: The Overlooked Singlet Oxygen Oxidation. *Chem. Eng. J.* **2020**, *388*, 124264.

(8) Guidotti, M.; Ravasio, N.; Psaro, R.; Gianotti, E.; Marchese, L.; Coluccia, S. Heterogeneous Catalytic Epoxidation of Fatty Acid Methyl Esters on Titanium-Grafted Silicas. *Green Chem.* **2003**, *5*, 421−424.

(9) Mirhashemi, F.; Amrollahi, M. Epoxidation of Vinyl Cyanides by Calcium Hypochlorite Under Catalyst-and Solvent-Free Conditions. *Tetrahedron Lett.* **2018**, *59*, 2661−2663.

(10) Ciriminna, R.; Albanese, L.; Meneguzzo, F.; Pagliaro, M. Hydrogen Peroxide: A Key Chemical for Today's Sustainable Development. *ChemSusChem* **2016**, *9*, 3374−3381.

(11) Grigoropoulou, G.; Clark, J.; Elings, J. Recent Developments on the Epoxidation of Alkenes Using Hydrogen Peroxide as an Oxidant. *Green Chem.* **2003**, *5*, 1−7.

(12) Cussó, O.; Cianfanelli, M.; Ribas, X.; Klein Gebbink, R. J. M.; Costas, M. Iron Catalyzed Highly Enantioselective Epoxidation of Cyclic Aliphatic Enones with Aqueous H_2O_2. *J. Am. Chem. Soc.* **2016**, *138*, 2732−2738.

(13) Huerta, I.; Biasi, P.; García-Serna, J.; Cocero, M. J.; Mikkola, J.-P.; Salmi, T. Continuous H_2O_2 Direct Synthesis Process: An Analysis of the Process Conditions That Make the Difference. *Green Process. Synth.* **2016**, *5*, 341−351.

(14) Schmidt, F. *Design of Supramolecular Nanocatalysts for the Biphasic Epoxidation of Olefins*, Ph.D. Dissertation, Technische Universität München, 2022.

(15) Ferreira, R.; Blesic, M.; Trindade, J.; Marrucho, I.; Lopes, J. N. C.; Rebelo, L. P. N. Solubility of Fluorinated Compounds in a Range

of Ionic Liquids. Cloud-Point Temperature Dependence on Composition and Pressure. *Green Chem.* **2008**, *10*, 918−928.
(16) Colomer, I.; Chamberlain, A. E.; Haughey, M. B.; Donohoe, T. J. Hexafluoroisopropanol as a Highly Versatile Solvent. *Nat. Rev. Chem.* **2017**, *1*, 1−12.
(17) Pozhydaiev, V.; Power, M.; Gandon, V.; Moran, J.; Lebœuf, D. Exploiting Hexafluoroisopropanol (HFIP) in Lewis and Brønsted Acid-Catalyzed Reactions. *Chem. Commun.* **2020**, *56*, 11548−11564.
(18) Kida, T.; Sato, S.-i.; Yoshida, H.; Teragaki, A.; Akashi, M. 1, 1, 1, 3, 3, 3-Hexafluoro-2-Propanol (HFIP) as a Novel and Effective Solvent to Facilely Prepare Cyclodextrin-Assembled Materials. *Chem. Commun.* **2014**, *50*, 14245−14248.
(19) Bhattacharya, T.; Ghosh, A.; Maiti, D. Hexafluoroisopropanol: The Magical Solvent for Pd-Catalyzed C−H Activation. *Chem. Sci.* **2021**, *12*, 3857−3870.
(20) Neimann, K.; Neumann, R. Electrophilic Activation of Hydrogen Peroxide: Selective Oxidation Reactions in Perfluorinated Alcohol Solvents. *Org. Lett.* **2000**, *2*, 2861−2863.
(21) Berkessel, A.; Krämer, J.; Mummy, F.; Neudörfl, J. M.; Haag, R. Dendritic Fluoroalcohols as Catalysts for Alkene Epoxidation with Hydrogen Peroxide. *Angew. Chem., Int. Ed.* **2013**, *52*, 739−743.
(22) Berkessel, A.; Adrio, J. A. Kinetic Studies of Olefin Epoxidation with Hydrogen Peroxide in 1, 1, 1, 3, 3, 3-Hexafluoro-2-Propanol Reveal a Crucial Catalytic Role for Solvent Clusters. *Adv. Synth. Catal.* **2004**, *346*, 275−280.
(23) Berkessel, A.; Adrio, J. A.; Hüttenhain, D.; Neudörfl, J. M. Unveiling the "Booster Effect" of Fluorinated Alcohol Solvents: Aggregation-Induced Conformational Changes and Cooperatively Enhanced H-Bonding. *J. Am. Chem. Soc.* **2006**, *128*, 8421−8426.
(24) Hollóczki, O.; Berkessel, A.; Mars, J.; Mezger, M.; Wiebe, A.; Waldvogel, S. R.; Kirchner, B. The Catalytic Effect of Fluoroalcohol Mixtures Depends on Domain Formation. *ACS Catal.* **2017**, *7*, 1846−1852.
(25) Wang, L.; Yuan, Q. Q.; Cao, W. J.; Han, J.; Zhou, X. G.; Liu, S. L.; Wang, X. B. Probing Orientation-Specific Charge-Dipole Interactions between Hexafluoroisopropanol and Halides: A Joint Photoelectron Spectroscopy and Theoretical Study. *J. Phys. Chem. A* **2020**, *124*, 2036−2045.
(26) Ghosh, D. A Quest for the Origin of Barrier to the Internal Rotation of Hydrogen Peroxide (H_2O_2) and Fluorine Peroxide (F_2O_2). *Int. J. Mol. Sci.* **2006**, *7*, 289−319.
(27) Shahi, A.; Arunan, E. Microwave Spectrum of Hexafluoroisopropanol and Torsional Behavior of Molecules with a CF_3−C−CF_3 Group. *J. Phys. Chem. A* **2015**, *119*, 5650−5657.
(28) Zhang, H. H.; Cao, W. J.; Yuan, Q. Q.; Zhou, X. G.; Valiev, M.; Kass, S. R.; Wang, X. B. Cryogenic "Iodide-Tagging" Photoelectron Spectroscopy: A Sensitive Probe for Specific Binding Sites of Amino Acids. *J. Phys. Chem. Lett.* **2020**, *11*, 4346−4352.
(29) Murray, J. S.; Politzer, P. Molecular Electrostatic Potentials and Noncovalent Interactions. *Wiley Interdiscip. Rev.: Comput. Mol. Sci.* **2017**, *7*, No. e1326.
(30) Gadre, S. R.; Suresh, C. H.; Mohan, N. Electrostatic Potential Topology for Probing Molecular Structure, Bonding and Reactivity. *Molecules* **2021**, *26*, 3289.
(31) Suresh, C. H.; Remya, G. S.; Anjalikrishna, P. K. Molecular Electrostatic Potential Analysis: A Powerful Tool to Interpret and Pedict Cemical Reactivity. *Wiley Interdiscip. Rev.: Comput. Mol. Sci.* **2022**, No. e1601.
(32) Lu, T.; Chen, F. Multiwfn: A Multifunctional Wavefunction Analyzer. *J. Comput. Chem.* **2012**, *33*, 580−592.
(33) Clark, T.; Murray, J. S.; Politzer, P. Role of Polarization in Halogen Bonds. *Aust. J. Chem.* **2014**, *67*, 451−456.
(34) Joseph, J.; Jemmis, E. D. Red-, Blue-, or No-Shift in Hydrogen Bonds: A Unified Explanation. *J. Am. Chem. Soc.* **2007**, *129*, 4620−4632.
(35) Sánchez-Sanz, G.; Trujillo, C.; Alkorta, I.; Elguero, J. Electron Density Shift Description of Non-Bonding Intramolecular Interactions. *Comput. Theor. Chem.* **2012**, *991*, 124−133.
(36) Solimannejad, M.; Malekani, M.; Alkorta, I. Cooperative and Diminutive Unusual Weak Bonding in $F_3CX\cdots HMgH\cdots Y$ and $F_3CX\cdots Y\cdots$ HMgH Trimers (X= Cl, Br; Y= HCN, and HNC). *J. Phys. Chem. A* **2010**, *114*, 12106−12111.
(37) Wang, J.; Gu, J.; Leszczynski, J. The Electronic Spectra and the H-Bonding Pattern of the Sulfur and Selenium Substituted Guanines. *J. Comput. Chem.* **2012**, *33*, 1587−1593.
(38) Bulat, F. A.; Murray, J. S.; Politzer, P. Identifying the Most Energetic Electrons in a Molecule: The Highest Occupied Molecular Orbital and the Average Local Ionization Energy. *Comput. Theor. Chem.* **2021**, *1199*, 113192.
(39) Sjoberg, P.; Murray, J. S.; Brinck, T.; Politzer, P. Average Local Ionization Energies on the Molecular Surfaces of Aromatic Systems as Guides to Chemical Reactivity. *Can. J. Chem.* **1990**, *68*, 1440−1443.

https://doi.org/10.1021/acs.jpclett.2c02237
J. Phys. Chem. Lett. 2022, 13, 8607−8612